AIMS Environmental Science

AIMS Environmental Science, 13(5): 865–895.
DOI: 10.3934/environsci.2026034
Received: 27 July 2026
Revised: 24 August 2026
Accepted: 15 September 2026
Published: 21 September 2026

https://www.aimspress.com/journal/environmental

Research article

Modeling heavy metal water-sediment partitioning using a nonlinear bifurcation approach

Livija Cveticanin[1,2], Vesna Gvoić[3,*], Dejan Krčmar[4], Aleksandra Tubić[4], Miodrag Zuković[1], Mihaela Timofti[5,6] and Miljana Prica[3]

[1] Department of Mechanics, Faculty of Technical Sciences, University of Novi Sad, Trg Dositeja Obradovića 6, 21000 Novi Sad, Serbia
[2] GAMF Faculty of Engineering and Computer Science, John von Neumann University, H-6000 Kecskemet, Izsak ut 10, Hungary
[3] Department of Graphic Engineering and Design, Faculty of Technical Sciences, University of Novi Sad, Trg Dositeja Obradovića 6, 21000 Novi Sad, Serbia
[4] Department of Chemistry, Biochemistry and Environmental Protection, Faculty of Sciences, University of Novi Sad, Trg Dositeja Obradovića 3, 21000 Novi Sad, Serbia
[5] Department of Applied Sciences, Cross-Border Faculty, Dunarea de Jos University of Galati, Str. Domnească, nr. 111, Galati, Romania
[6] REXDAN Research Infrastructure, Dunarea de Jos University of Galati, Str. Domnească, nr. 111, Galati, Romania

* **Correspondence:** Email: kecic@uns.ac.rs; Tel: +381214852554.

Abstract: Heavy metal transport between the water column and sediment is commonly described using linear or empirical relationships, which may not capture nonlinear feedback mechanisms and abrupt changes in contamination states. In this study, we proposed a nonlinear cubic equilibrium model for describing metal partitioning between water and sediment and for identifying critical transition conditions associated with bifurcation behavior.

The proposed model established a nonlinear relationship between the input metal concentration in water I_i and the accumulated sediment concentration C_i. Using experimental data for copper (Cu) and nickel (Ni) transport from the literature data, model parameters were estimated by the least-squares method. The obtained response curves exhibited an S-shaped structure, indicating the existence of

multiple equilibrium states, bistability, and hysteresis. Fold points obtained from the condition $dI_i/dC_i = 0$ defined critical thresholds at which saddle-node bifurcations occur and abrupt transitions between contamination states become possible.

The bifurcation analysis with respect to the nonlinear parameter p_i further identified critical values separating bistable and monostable regimes. The results demonstrated that Cu and Ni systems may exhibit history-dependent behavior, where the sediment contamination level is not determined solely by the current pollution input but also by the previous evolution of the system.

The proposed framework extends conventional pollutant transport models by incorporating nonlinear dynamics, multistability, and regime-shift mechanisms. It provides a mathematical basis for identifying tipping points in water-sediment contamination systems and offers a potential tool for assessing environmental risks associated with sudden changes in metal accumulation.

The main contribution of this work is the demonstration that nonlinear bifurcation analysis provides insight into critical states, multistability, hysteresis, and regime transitions in water-sediment contamination systems, extending conventional concentration-based approaches toward a deeper understanding of nonlinear environmental dynamics.

Keywords: heavy metal transport; water-sediment interaction; nonlinear cubic model; bifurcation analysis; saddle-node bifurcation; hysteresis; multistability; tipping point; regime shifts; sediment contamination

1. Introduction

Surface water quality assessment is a critical component of environmental management, providing the basis for policy decisions, pollution control, and ecosystem protection. Over the past decades, a variety of numerical, statistical, and machine learning models have been developed to evaluate water quality and to simulate the transport, transformation, and fate of pollutants in aquatic systems. Classical numerical models such as AQUATOX, CE-QUAL-W2, EFDC, MIKE, and WASP are widely used for predicting chemical and biological processes, including nutrient cycling, dissolved oxygen dynamics, and contaminant transport [1,2]. These tools enable researchers and managers to model complex interactions in surface waters, supporting informed decision-making regarding pollution mitigation and ecosystem restoration.

Catchment-scale models further integrate hydrological, sediment, and erosion processes, providing insight into pollutant loads at the watershed level [3]. Statistical and econometric approaches, including vector autoregressive (VAR) models and multivariate analyses, have been applied to evaluate the influence of sediment-related factors on water quality trends and pollutant sources [4,5]. Recently, machine learning (ML) and artificial intelligence (AI) frameworks have emerged as powerful tools for predictive water quality modeling, particularly in addressing incomplete datasets and complex non-linear relationships. Approaches such as random forest, artificial neural networks, and transfer learning have been successfully used to predict heavy metal pollution, suspended solids, and sediment risk indices in urban rivers and seaports [6–9].

Indices-based methods, including Water Quality Indices (WQI), Heavy Metal Indices (HMI), and trophic status indicators, remain an important component of water quality evaluation, often combined with statistical or ML models to quantify pollution levels and source contributions [1,10]. Collectively, these modeling frameworks provide a comprehensive toolkit for ranking water bodies by pollution severity and identifying priority areas for intervention. By reviewing the evolution, capabilities, and applications of these models, we aim to provide a systematic foundation for selecting appropriate approaches for water quality ranking in diverse aquatic environments.

Despite this extensive development, several limitations remain in methodologies. Classical numerical models (e.g., AQUATOX, CE-QUAL-W2, EFDC, MIKE, WASP) provide detailed mechanistic simulations but often require extensive calibration data and are limited in their ability to capture non-linear threshold behaviors, such as sudden shifts in pollutant dynamics [1,2]. Statistical and ML approaches can handle large datasets and incomplete measurements, yet they frequently act as "black boxes" providing limited interpretability regarding the underlying physico-chemical processes [6–8]. Furthermore, most models focus on predicting pollutant concentrations or indices without explicitly analyzing dynamic stability, bifurcations, or temporal non-linearities in water quality behavior.

Building on the reviewed models, we propose a nonlinear mathematical framework for describing heavy metal partitioning between the water column and sediment. The proposed approach introduces a cubic nonlinear equilibrium model capable of incorporating feedback effects, saturation mechanisms, and threshold-dependent accumulation processes. Unlike conventional empirical or data-driven approaches, the nonlinear formulation provides insight into the stability structure of the system, enabling the identification of equilibrium branches, bifurcation points, and possible abrupt transitions between contamination states.

A nonlinear bifurcation-based description provides not only quantitative prediction of sediment contamination levels but also qualitative information about the system regime, including monostable, bistable, and critical states. Such an approach establishes a connection between mechanistic environmental processes and nonlinear systems theory, providing a framework for analyzing hidden instability mechanisms that cannot be identified using traditional pollution indices or regression models.

Pollution indices and statistical approaches are useful for ranking contamination levels; however, they do not describe the mechanisms controlling pollutant accumulation or explain why sudden changes in contamination states may occur. The proposed nonlinear model establishes a direct relationship between the external pollution input, sediment accumulation, and system stability, thereby providing a mechanistic interpretation of observed contamination patterns.

Beyond improving the understanding of nonlinear water-sediment interactions, the proposed framework may provide a theoretical basis for identifying critical changes in heavy-metal partitioning that could be relevant to sediment remediation. This perspective may also be useful for remediation technologies, including solidification/stabilization (S/S), whose primary objective is the long-term reduction of metal mobility.

The main contribution of this study is the development of a nonlinear bifurcation-based framework capable of revealing multistable contamination states in water–sediment systems. Unlike

conventional approaches that assume a unique relationship between pollution intensity and sediment concentration, the proposed model demonstrates that the same level of external pollution input may correspond to different sediment contamination states due to nonlinear feedback mechanisms and the history of system evolution.

By applying bifurcation analysis, the proposed framework identifies critical parameter values and fold points associated with transitions between monostable and bistable regimes. These critical conditions provide a mathematical basis for predicting possible tipping points, where relatively small changes in system parameters may lead to abrupt shifts between contamination states.

The applicability and generality of the proposed approach are demonstrated through two independent case studies involving Cu and Ni transport. The results show that multistability, hysteresis, and regime shifts are not specific to a particular metal but arise from the intrinsic nonlinear structure of the water–sediment interaction mechanism.

Furthermore, we establish a connection between environmental pollutant transport and nonlinear dynamical systems theory by introducing concepts such as saddle-node bifurcations, hysteresis, and stability transitions into the analysis of heavy metal accumulation processes. Therefore, the proposed approach extends beyond conventional curve fitting and provides a predictive framework for identifying critical thresholds, hidden instability mechanisms, and potential abrupt transitions in aquatic pollution dynamics. Such a framework may contribute to the development of early-warning indicators and improved decision-support tools for environmental management.

The novelty of this work lies in introducing a nonlinear bifurcation-based framework for water–sediment heavy-metal partitioning that goes beyond the conventional estimation of concentration relationships. In contrast to linear or purely empirical models, the proposed approach explicitly identifies equilibrium branches, bistable regions, fold (saddle-node) bifurcations, hysteresis intervals, and critical pollution thresholds. The framework is further applied to Cu and Ni to demonstrate how these mathematical features can be translated into site-specific contamination-risk zones and early-warning thresholds. Thus, the main contribution is not only to describe the nonlinear relationship between aqueous and sediment metal concentrations, but also to identify conditions under which the system may undergo abrupt and history-dependent transitions.

The paper is organized into five sections. Following this introduction, in Section 2, we analyze the case of constant pollution source with linear sediment uptake. In Section 3, we present the theoretical development of the constant pollution source with nonlinear sediment uptake model, which represents the central part of this study. In Section 4, the theoretical results are applied to two case studies involving Cu and Ni concentration. In Section 5, we provide a discussion of the obtained results, followed by the conclusions of the study.

2. Constant pollution source and linear sediment uptake

Assume that the pollution source contains a constant concentration of heavy metals and that the sediment uptake process is linear. Neglecting diffusion and nonlinear effects, the governing equation becomes:

$$\frac{dC_i}{dt} = I_i - k_i C_i \tag{1}$$

where C_i denotes the concentration of a heavy metal in sediment, k_i is the resuspension coefficient that characterizes the mobility and removal rate of the heavy metal from the sediment, and I_i = const. represents the constant input concentration of the corresponding metal from the pollution source. The first term describes the continuous supply of metal to the sediment, whereas the second term represents the natural removal or release process.

Integrating Eq. (1) under the initial condition $C_i(0) = C_{i0}$ gives:

$$C_i = \frac{I_i}{k_i}(1 - \exp(-k_i t)) + \exp(-k_i t) C_{i0} \tag{2}$$

Solution (2) describes the temporal evolution of heavy metal concentration in the sediment and provides information about the contamination rate and the characteristic time required for the system to approach equilibrium.

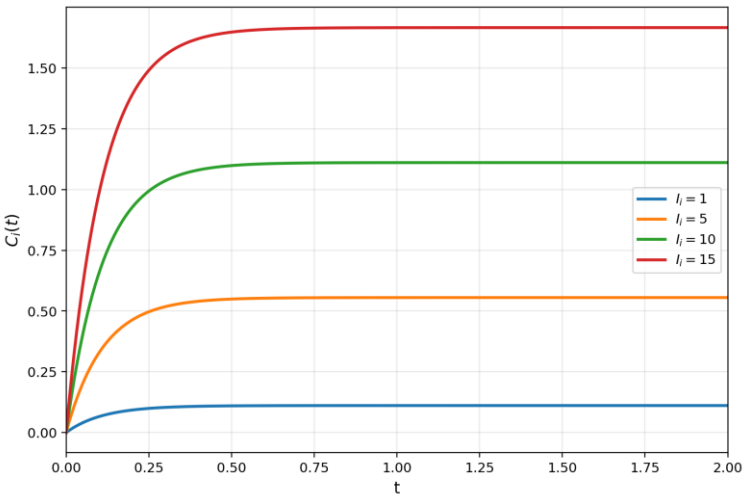


Figure 1. Variation of the metal concentration C_i in the sediment over time for different metal concentrations I_i in the water.

Analysis of Eq. (2) shows that the transfer of heavy metals from water to sediment depends on sediment properties, metal characteristics, and pollution intensity I_i. For sufficiently long times, when $t \to \infty$, the transient term vanishes and the concentration approaches the steady-state value

$$C_i^* = \frac{I_i}{k_i} = const. \tag{3}$$

Equation (3) demonstrates that the final concentration of heavy metals in the sediment is independent of the initial contamination level. Instead, the equilibrium state is determined by the

balance between the external metal input and the natural removal processes. Therefore, within the framework of the linear model, the relationship between the metal concentration in water and sediment is proportional.

Figure 1 illustrates the temporal evolution of heavy metal concentration in sediment C_i (see (2)) for different values of the input metal concentration in the water I_i. The initial metal concentration in sediment was assumed to be $C_{i0} = 0$, while the model parameter was set to $k_i = 9$. As shown in the Figure 1, the concentration in the sediment rapidly approaches its steady-state value, with the transient phase being slightly shorter for lower values of I_i. The steady-state metal concentration in the sediment is given by Eq. (3).

Since heavy metal concentrations in water are commonly expressed in [mg/L], whereas sediment concentrations are expressed in [mg/kg], a normalization factor a_i is introduced to relate the input term I_i to the water concentration C_{wi}: $I_i = a_i C_{wi}$. For $a_i = 1[\frac{L}{kg}]$, Eq. (3) becomes:

$$C_{si} = \frac{C_{wi}}{k_i} = const. \tag{4}$$

In environmental sciences, the reciprocal value of the parameter k_i is commonly used and defined as the partition (distribution) coefficient K_{di}:

$$K_{di} = \frac{C_{s0i}}{C_{wi}} \tag{5}$$

where the dimension of K_{di} is [L/kg].

The distribution coefficient K_{di} is widely applied in hydrogeology, sediment transport studies, and ecotoxicological assessments. Its value depends on several environmental factors, including sediment composition, pH, organic matter content, temperature, and physicochemical properties of the metal. Comparison of K_{di} values among metals provides a useful criterion for evaluating their accumulation potential. A larger K_{di} indicates stronger metal retention and accumulation in sediment, whereas a smaller value corresponds to weaker transfer from water to sediment.

Although the linear approach is practical and often provides satisfactory first-order estimates, natural aquatic systems exhibit considerably more complex behavior. In real environments, changes in sediment contamination are not necessarily proportional to variations in the incoming metal concentration. Several nonlinear mechanisms, such as adsorption saturation, competitive interactions among metals, changes in particle characteristics, and chemical transformations, may influence the accumulation process.

For example, by analyzing the experimental data reported by Shanbehzadeh et al. [11], coefficient k_i can be estimated from measured water and sediment concentrations. If the metal concentration in water changes, Eq. (4) predicts a proportional change in sediment concentration. However, using the experimentally obtained coefficient k_i, the predicted value may differ significantly from newly measured sediment concentrations. This discrepancy indicates that the relationship between water and sediment contamination cannot always be represented by a linear law.

When experimental data are available only at discrete concentration levels, linear interpolation is used to estimate intermediate values between two consecutive measured data points. The interpolation is introduced only to facilitate the comparison and visualization of the experimental data and model predictions and does not provide additional experimental information. Linear interpolation was selected because it provides a simple and transparent connection between consecutive measurements without introducing artificial local maxima or minima. Nevertheless, it may affect the detailed shape of the concentration–concentration relationship, particularly when the experimental data are sparse or exhibit pronounced nonlinear variation. Therefore, the interpolated values are interpreted only within the resolution of the available experimental measurements.

For this reason, increased monitoring frequency is recommended in the vicinity of the predicted branching (bifurcation) threshold, where small changes in the input concentration may produce substantial changes in the sediment response. More closely spaced experimental measurements in this region would reduce the uncertainty associated with linear interpolation and provide a more reliable basis for identifying abrupt transitions and bifurcation behavior.

Moreover, experimental observations show that variations in water metal concentration may induce abrupt changes in sediment concentration, either from a lower to a higher contamination state or vice versa [12]. Similar jump phenomena are well known in nonlinear mechanical systems, particularly in cubic Duffing-type models, where sudden transitions between stable states may occur due to nonlinear feedback mechanisms [13]. By analogy, it is hypothesized that an analogous nonlinear framework may be appropriate for describing transitions in sediment contamination as a function of water metal concentration.

Finally, field observations confirm that heavy metal accumulation in sediments often exhibits pronounced nonlinear characteristics that cannot be captured by the linear uptake model. Feedback processes associated with adsorption mechanisms, particle interactions, chemical equilibrium, and saturation effects may lead to deviations from proportional behavior. These observations motivate the extension of the framework toward a nonlinear dynamical model capable of describing complex environmental responses, including possible multiple equilibrium states and abrupt contamination transitions.

3. Materials and methods

3.1. Constant pollution source and nonlinear sediment uptake

Assuming that the pollution source maintains a constant concentration of heavy metals, the sediment uptake process is described by a nonlinear dynamical model. Unlike the linear formulation, this model incorporates nonlinear accumulation and saturation effects, which are frequently observed in environmental systems. The model is written as:

$$\frac{dC_i}{dt} = I_i - k_i C_i + q_i C_i^2 - p_i C_i^3 \tag{6}$$

where C_i denotes the concentration of a heavy metal in sediment [mg/kg], I_i is the concentration of the metal introduced by wastewater or polluted water [mg/L], $k_i\, C_i$ represents removal and

resuspension processes, $q_i C_i^2$ describes nonlinear accumulation mechanisms (e.g., autocatalytic enhancement of metal retention), and $p_i C_i^3$ accounts for saturation effects.

The cubic functional form in Eq. (6) is introduced as the lowest-order polynomial representation capable of describing nonlinear enhancement and saturation of sediment metal accumulation. The linear term, $-k_i C_i$ represents the first-order removal or resuspension process, while the positive quadratic term $q_i C_i^2$, accounts for concentration-dependent enhancement of metal retention. At higher sediment concentrations, the negative cubic term, $-p_i C_i^3$, becomes dominant and limits further accumulation, thereby representing saturation or a decrease in the net accumulation rate. Consequently, the competition between the quadratic enhancement and cubic saturation terms can produce a nonlinear equilibrium relation with multiple equilibrium states and, under appropriate parameter conditions, bifurcation behavior. The cubic model is therefore used as a reduced-order phenomenological representation of the competing accumulation and limiting mechanisms rather than as a direct derivation from a single microscopic adsorption mechanism.

The quadratic term represents positive feedback mechanisms associated with enhanced adsorption, cooperative sorption processes, bioaccumulation, and particle interactions. The cubic term introduces saturation effects caused by the finite capacity of sediment binding sites, preventing unlimited accumulation at high contamination levels. Such nonlinear formulations are widely employed in reaction–diffusion systems, ecological dynamics, and adsorption kinetics to describe feedback-driven growth and saturation effects. Consequently, Eq. (6) provides a physically motivated framework that incorporates deposition, resuspension, nonlinear sorption, and saturation within a single dynamical model.

The nonlinear structure of Eq. (6) is consistent with developments in adsorption science and complex environmental systems, where nonlinear feedback mechanisms and multistability have been increasingly reported. Modern adsorption isotherm modeling emphasizes that heterogeneous surface interactions and cooperative effects can lead to nonlinear accumulation dynamics that cannot be captured by classical linear models [14]. In particular, comprehensive reviews of adsorption isotherms highlight the importance of nonlinear parameterizations in describing real environmental systems with complex sorption behavior and competing processes [14,15].

Furthermore, studies in complex systems ecology demonstrate that environmental systems under resource or pollutant stress may exhibit abrupt regime shifts, hysteresis, and bistability due to nonlinear feedback loops and threshold dynamics [16,17]. These observations provide a physical motivation for interpreting the quadratic and cubic terms as effective representations of cooperative accumulation and saturation mechanisms.

Eq. (6) thus simultaneously incorporates deposition, resuspension, nonlinear sorption, and saturation effects. Parameters k_i, q_i, and p_i represent effective linear and nonlinear interactions governing the transfer and accumulation of heavy metals in sediment. Their values are determined by fitting the model to experimental sediment-water concentration data. This is typically performed using nonlinear regression techniques, most commonly nonlinear least squares optimization, which minimizes the deviation between measured and modeled concentrations over time. When site-specific data are limited, parameter values can also be adopted from literature studies reporting similar sediment types, environmental conditions, and metal species.

The nonlinear feedback structure of the system suggests the possible emergence of multiple stable equilibrium states under the same external forcing conditions. This implies that the system may exhibit multistability, where different long-term contamination levels coexist depending on initial conditions. As a consequence, small changes in the control parameters may trigger abrupt regime shifts between low and high contamination states, indicating the presence of potential bifurcation behavior.

3.1.1. Environmental controls and scope of the reduced-order model

The proposed cubic formulation is intentionally developed as a reduced-order model in which the effects of several physicochemical processes are represented through effective parameters rather than through explicitly resolved environmental variables. In natural aquatic systems, metal partitioning between the water column and sediment is affected by pH, total organic carbon (TOC), sediment particle size and mineralogy, Fe/Mn oxyhydroxides, competing metal ions, redox conditions, temperature, and hydrodynamic processes such as resuspension and deposition. These factors may modify the availability of adsorption sites, metal speciation, desorption rates, and the effective nonlinear feedback associated with sediment accumulation.

Accordingly, parameters k_i, q_i, and p_i should not be interpreted as universal constants for a given metal. Rather, they represent effective, site- and condition-dependent parameters that implicitly incorporate the combined influence of the environmental processes not explicitly resolved in the present formulation. Changes in pH or redox conditions, for example, may alter metal speciation and adsorption affinity, whereas variations in TOC, particle size, and Fe/Mn oxyhydroxide content may modify the effective retention capacity of the sediment. Similarly, competing metal ions and hydrodynamic resuspension may change the apparent balance between accumulation and removal.

This model therefore does not attempt to replace a fully mechanistic geochemical or hydrodynamic model. Its purpose is to identify whether the observed water–sediment relationship can exhibit nonlinear response, multiple equilibria, hysteresis, and critical transition thresholds. The identified bifurcation boundaries should consequently be interpreted as conditional thresholds valid for the environmental state represented by the calibration data. For application to other sites or substantially different environmental conditions, the effective parameters should be recalibrated using site-specific measurements.

This reduced-order formulation also provides a basis for future model extensions in which selected environmental variables, such as pH, TOC, redox potential, suspended sediment concentration, or seasonal hydrodynamic forcing, can be introduced as additional control parameters. Such an extension would enable the position and width of the bistable region to be evaluated under changing environmental conditions.

3.2. Stationary states: number and existence

For stationary conditions, $\frac{dC_i}{dt} = 0$, Eq. (6) becomes:

$$f(C_i) = I_i - k_i C_i + q_i C_i^2 - p_i C_i^3 \tag{7}$$

and therefore:

$$I_i - k_i C_i + q_i C_i^2 - p_i C_i^3 = 0 \tag{8}$$

The solutions of the cubic equation (8) define the stationary concentrations of heavy metals in sediment. Since Eq. (8) may possess either one or three real roots, the system can exhibit either one or three stationary states.

The number of real roots is determined by the discriminant of the cubic equation. To evaluate the discriminant, introduce the transformation:

$$C_i = y + \frac{q_i}{3p_i} \tag{9}$$

which yields:

$$y^3 + Py + Q = 0 \tag{10}$$

where $P = \frac{3p_i k_i - q_i^2}{3p_i^2}$, $Q = \frac{2q_i^3 - 9p_i k_i q_i + 27p_i^2 I_i}{27p_i^3}$

The discriminant of Eq. (10) is:

$$\Delta = (\frac{Q}{2})^2 + (\frac{P}{3})^3 \tag{11}$$

Analysis of the discriminant leads to the following conclusions:

- For $\Delta > 0$, Eq. (8) has one real stationary solution and two complex conjugate roots.
- For $\Delta < 0$, there exist three real stationary solutions.
- $\Delta = 0$ represents the bifurcation (critical) curve at which two roots merge.

Although the bifurcation condition can be expressed through Eq. (11), its analytical interpretation is cumbersome. Therefore, an alternative and more physically transparent formulation is introduced.

3.3. Transient evolution toward steady states

In the bistable regime, where Eq. (8) possesses three real solutions, the transient evolution can be obtained by factorizing the cubic polynomial. To determine the transient time evolution, Eq. (6) is rewritten in the form:

$$\frac{dC_i}{C_i^3 - \frac{q_i}{p_i} C_i^2 + \frac{k_i}{p_i} C_i - \frac{I_i}{p_i}} = -p_i dt \tag{12}$$

i.e.,

$$\sum_{j=1}^{3} \frac{A_j}{(C_i - C_j)} dC_i = -p_i dt \tag{13}$$

when $C_{j,}, j = 1,2,3,$ are the three real solutions of (13), and A_j , $j = 1,2,3,$ are three corresponding constants. After integration for the initial condition $C_i(0) = C_{i0}$, the solution is:

$$\sum_{j=1}^{3} A_j \ln \left| \frac{C_i - C_j}{C_{i0} - C_j} \right| = -p_i t \tag{14}$$

where A_j for $j = 1,2,3,$ are constant. After some modification of (14) the implicit form of concentration variation is:

$$\prod_{j=1}^{3} \left| \frac{C_i - C_j}{C_{i0} - C_j} \right|^{A_j} = \exp(-p_i t) \tag{15}$$

Equation (15) describes the transient evolution of the metal concentration in the sediment as a function of the metal concentration in the water. In the long-time limit, the system approaches one of the possible steady-state values C_j. The selected equilibrium state depends not only on the current pollution level but also on the pollution history, indicating the presence of path-dependent behavior and possible hysteresis effects.

Equation (15) provides the mathematical trajectory toward an equilibrium state for a prescribed constant input and initial condition; however, it does not constitute a calibrated prediction of the duration of a real environmental regime shift. In particular, the available measurements consist of discrete sampling campaigns rather than a sufficiently resolved time series covering a transition between alternative stable states. Therefore, the dataset does not enable reliable estimation of transition duration or jump velocity.

The transient formulation should consequently be interpreted as a theoretical description of relaxation toward equilibrium rather than as a quantitative prediction of the rate of an environmental tipping event. Quantification of transition duration would require time-resolved measurements of water and sediment metal concentrations, together with hydrodynamic and physicochemical variables. Such observations could subsequently be used to calibrate a fully dynamic version of the proposed model.

3.4. Determination of the bifurcation curve

Differentiating Eq. (7) with respect to C_i gives:

$$f'(C_i) = 3p_i C_i^2 - 2q_i C_i + k_i \tag{16}$$

For (16) equal to zero yields:

$$3p_i C_i^2 - 2q_i C_i + k_i = 0 \tag{17}$$

with solutions:

$$C_{ib}^{1,2} = \frac{q_i \pm \sqrt{q_i^2 - 3p_i k_i}}{3p_i} \tag{18}$$

The second derivative of the function given by Eq. (7) is $f^{"}(C_i) = 6p_i C_i - 2q_i$, This function is used to determine the extrema of the steady-state solutions given by Eq. (18). If the value of $f^{"}(C_i)$ at C_{ib}^1 is negative, the corresponding solution represents a local maximum, whereas if $f^{"}(C_i)$ is positive, the solution C_{ib}^1 corresponds to a local minimum. Consequently, the coordinates of the local minimum and maximum points are denoted as (I_{ib}^1, C_{ib}^1) and (I_{ib}^2, C_{ib}^2), where $I_{ib}^1 = k_i C_{ib}^1 - q_i (C_{ib}^1)^2 + q_i (C_{ib}^1)^3$ and $I_{ib}^2 = k_i C_{ib}^2 - q_i (C_{ib}^2)^2 + q_i (C_{ib}^2)^3$. In other words, the points defined by Eq. (18) correspond to the local maximum and local minimum of the steady-state response function. These points represent the critical states at which the system changes its stability characteristics and may exhibit abrupt transitions between steady-state metal concentrations. The condition for the existence of three stationary states, corresponding to one local maximum and one local minimum of the steady-state function, is:

$$q_i^2 - 3p_i k_i > 0 \tag{19}$$

whereas:

$$q_i^2 - 3p_i k_i < 0 \tag{20}$$

Indicates that Eq. (8) has no extrema and therefore only one stationary solution exists. Consequently, the necessary condition for bistability is given by Eq. (19), namely.

When a stationary point simultaneously satisfies the condition for an extreme, it becomes a bifurcation point. Mathematically, the bifurcation concentration C_{ib} is determined by the conditions

$$f(C_{ib}) = 0, \qquad f'(C_{ib}) = 0 \tag{21}$$

Expressing k_i from Eq. $(21)_2$ and substituting it into Eq. $(21)_1$ gives:

$$k_i = -3p_i C_{ib}^2 + 2q_i C_{ib}, \qquad I_i = C_{ib}(q_i - 2p_i C_{ib}^2). \tag{22}$$

Equations (22) represent the parametric form of the bifurcation curve. Using the critical concentrations defined by Eq. (18), the upper and lower limits of the hysteresis region are obtained as:

$$I_{i1} = C_{ib1}(q_i - 2p_i C_{ib1}^2), \qquad I_{i2} = C_{ib2}(q_i - 2p_i C_{ib2}^2) \tag{23}$$

The region enclosed by these curves corresponds to the bistable domain, where three stationary states coexist, whereas outside this region only one stationary state exists. Therefore, the occurrence of bifurcation requires the fulfillment of condition (19), which ensures the existence of two real roots of Eq. (17).

By eliminating the parameter C_{ib} from Eqs. (22), the implicit curve in the (I_i, p_i) parameter plane is obtained. This curve separates the region with a single stationary state from the region where three stationary states exist. It represents the boundary of a fold (saddle-node) bifurcation.

Remark: The conditions Δ=0 and Eq. (22) describe the same bifurcation curve, expressed in two

different mathematical forms. For ecological applications, the parametric representation given by Eq. (22) is more convenient because it allows direct visualization of the bifurcation structure in the (p_i, I_i) parameter plane.

3.5. Critical bifurcation point

Of particular importance is the determination of the critical bifurcation point. It occurs when $q_i^2 = 3p_i k_i$, i.e., when the two solutions of Eq. (17) coincide. Substituting $C_{ib} = q_i/3p_i$ into (18) yields:

$$I_{icr} = \frac{q_i^2}{3p_i}(1 - \frac{2q_i}{9p_i}) \tag{24}$$

Finally, it is concluded that the tipping point leads to a sudden transition to a highly polluted state, while hysteresis implies a strong irreversibility in returning to the previous state. Equation (20) defines the critical value of the input metal pollution. This value represents an ecological "tipping point" or critical transition threshold.

3.6. Stability of stationary states

For stationary states C_i^*, which are solutions of the cubic equation, stability is determined by evaluating the derivative of the function $f'(C_i^*)$. The following holds:

If $f'(C_i^*)>0$, the stationary state is unstable.

If $f'(C_i^*)<0$, the stationary state is stable.

For three real roots, the lower and upper branches are stable, while the middle branch is unstable. This has a clear physical interpretation:

For small I_i, there exists a single stable state with low contamination.

When I_i reaches a critical value, two stationary states merge and the system becomes unstable.

Beyond this threshold, the system abruptly transitions to a high-contamination stable state.

Such abrupt transitions are commonly referred to as critical transitions or "tipping effects." While perturbations are small, the system returns to its original state. However, once the critical point (tipping point) is crossed, the system undergoes an abrupt transition toward an alternative stable state.

3.7. Sampling and analysis

The model was validated using water and sediment samples collected during sampling campaigns conducted in October 2024 and May 2025 within the Novi Sad-Savino Selo section of the Danube-Tisa-Danube (DTD) Canal, Serbia. The sediment samples were dried at 105°C and subsequently subjected to microwave-assisted acid digestion according to USEPA Method 3051A [18]. The pseudo-total concentrations of Ni and Cu in the in the sediment and water samples were determined according to USEPA Methods 7000B [19] and 7010 [20].

Quality assurance and quality control (QA/QC) procedures were implemented throughout the analytical process to ensure the accuracy and precision of the measurements. Method blanks were

processed together with the samples to assess potential contamination during sample preparation and analysis. Duplicate analyses were performed to evaluate analytical precision, with relative standard deviations (RSD) of 4% for Ni and 7,37% for Cu. The accuracy of the analytical procedure was assessed using a certified reference material (CRM), "Metals in soil" - SQC001-30G Lot No LRAC9394, subjected to the same digestion and analytical procedures as the sediment samples. Recoveries of Ni and Cu were 98,17% and 99,44%, respectively. Instrument calibration was performed using appropriate multi-point calibration standards, and calibration verification standards were analyzed periodically to confirm instrument stability. The limits of detection (LOD) and limits of quantification (LOQ), determined under the applied analytical conditions, were 0,011 and 0,023 mg/kg for Ni and 0,012 and 0,025 mg/kg for Cu, respectively. Metal concentrations in the method blanks were below the corresponding detection limits. These QA/QC results confirmed satisfactory accuracy, precision, and absence of significant contamination during sample preparation and instrumental analysis [19].

4. Application of the model to determine the relationship between heavy metal concentrations in water and sediment

To demonstrate the applicability of the proposed theoretical framework, mathematical models were constructed using experimental data reported in the literature. These models were developed in accordance with the proposed nonlinear theory and were used to investigate the contamination state as well as the influence of changes in heavy metal concentration in water on the corresponding concentration in the sediment. Two case studies were analyzed. The first considered Cu and the second Ni in the South Saskatchewan River, using the experimental data reported by Prajapati et al. [12]. In addition, the previously developed models, based on measurements obtained at the Danube-Tisa-Danube (DTD) Canal, at the Novi Sad-Savino Selo section near Rumenka, Serbia, before 2024, were shown to accurately reproduce the newly measured Cu and Ni concentrations in water and sediment collected at the same location, confirming their predictive capability.

4.1. Modeling the distribution of Cu in water and sediment based on experimental data

Using the procedure described above, a mathematical model was developed based on the experimental data reported by Prajapati et al. [12] for Cu transport in the South Saskatchewan River. The measured concentration pairs (I_i, C_i) for Cu were (0.1, 0.3), (0.3, 0.5), (0.25, 1.5), and (1.8, 3), with units of ($\mu g/L$, mg/kg). The measured data indicate that the first two points belong to the lower branch of the response curve, whereas the remaining two points lie on the upper branch. This distribution suggests the existence of a nonlinear multivalued relationship between heavy metal concentrations in water and sediment, which is consistent with bistable system behavior predicted by the proposed model.

Using the least squares method, the following cubic relationship is obtained:

$$I_i - 1.0309C_i + 0.97C_i^2 - 0.27C_i^3 = 0 \tag{25}$$

Figure 2 presents the response curve $C_i(I_i)$ obtained from Eq. (25) together with the experimental

data. The measured concentration pairs are close to the predicted curve, indicating good agreement between the nonlinear model and the experimental observations.

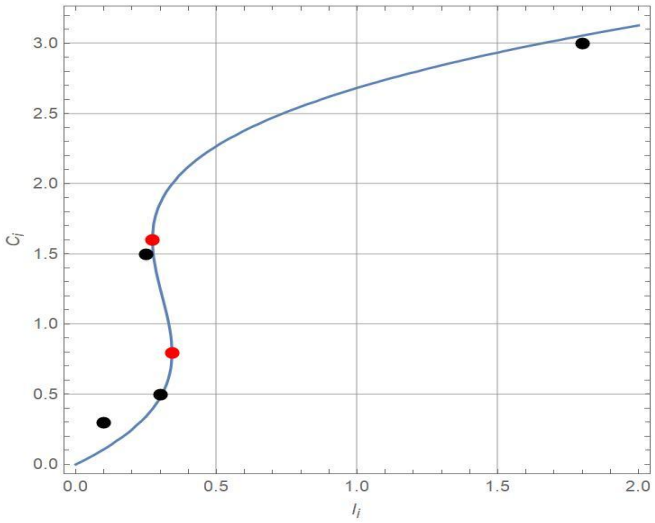


Figure 2. Response curve $C_i(I_i)$ for Cu with the measured data (black points) and the predicted critical bifurcation points (red points).

Table 1 compares the measured Cu concentrations in water I_{im} with the calculated values I_i obtained for the prescribed sediment concentrations C_i The relative error $I_{ierr} = \left|\frac{I_i - I_{im}}{I_i}\right|$ was calculated to quantify the deviation between the measured and modeled values. The results show that the differences between the measured and calculated concentrations are relatively small, with the maximum error not exceeding 16%.

Table 1. Comparison of measured and calculated Cu concentrations in water.

C_i	I_{im}	I_i	I_{ierr}
0.3	0.10	0.1192	0.1610
0.5	0.30	0.3067	0.0196
1.5	0.25	0.2751	0.0912
3.0	1.8	1.5527	0.0891

The $C_i(I_i)$ diagram shown in Figure 2 exhibits an S-shaped response curve. Such behavior indicates the possibility of bifurcation and abrupt transitions between different sediment contamination states as the Cu concentration in water increases. Parameter p_i was selected as the bifurcation control parameter. Figure 3 presents the $C_i(I_i)$ diagrams for different values of p_i.

As can be observed, increasing p_i gradually reduces the nonlinear character of the response curve. The S-shaped structure becomes progressively smoother and transforms into a monotonic curve without extrema. Therefore, determining the critical value of p_i at which the bifurcation structure disappears, is of particular importance.

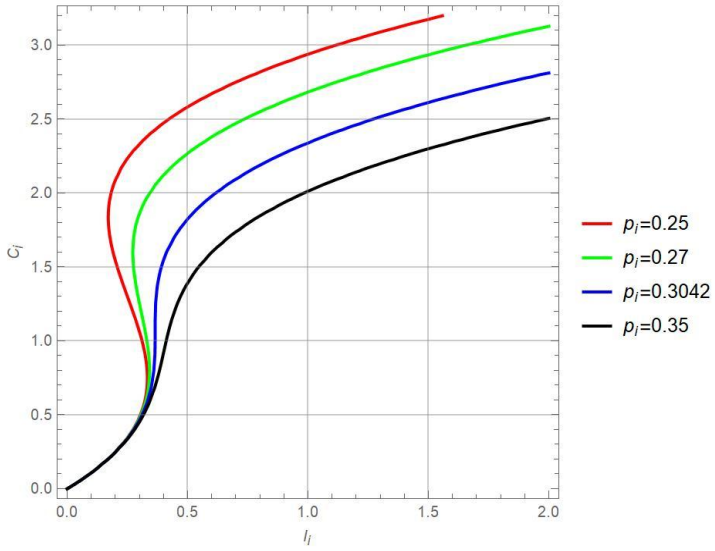


Figure 3. Influence of the parameter p_i on the $C_i(I_i)$ response curve for Cu.

4.1.1. Critical points and multistability

Using the condition dI_i/dC_i=0 obtained from the Eq. (25), the extremal values of the function $I_i(C_i)$ were calculated and are presented in Table 2.

Table 2. Calculated extremal values of the input Cu concentration I_i and corresponding sediment concentrations C_i.

Type	C_{ib}	I_{ib}
Local maximum	0.79583	0.34216
Local minimum	1.59923	0.27216

These critical points are also shown in Figure 2. The calculated values define distinct regions characterized by different numbers of real stationary solutions:

For $I_i > 0.342166$ - one real solution;

For $0.27216 \leq I_i \leq 0.34216$ - three real solutions;

For $I_i < 0.27216$ - one real solution.

Therefore, a bistable (hysteretic) region exists within the interval $0.27216 \leq I_i \leq 0.34216$ where the system can exhibit abrupt transitions between different steady states. Specifically, the transition from one to three stationary solutions occurs at I_i =0.34216, whereas the reverse transition from three to one stationary solution occurs at I_i =0.27216. The width of the hysteresis interval is therefore ΔI_i =0.342166−0.272160=0.070006. This hysteresis width represents the range of input metal concentrations over which multiple stationary sediment contamination states coexist.

4.1.2. Bifurcation interpretation

The bifurcation structure can also be analyzed using the parameterized form:

$$3p_i C_i^2 - 1.94C_i + 1.0309 = 0 \tag{26}$$

This defines the fold (saddle-node) bifurcation curve in the (p_i, C_i) plane. In Figure 4, the bifurcation diagram $C_i(p_i)$ is plotted. The bifurcation diagram $C_i(p_i)$ shows the set of critical points where the system loses uniqueness of solutions.

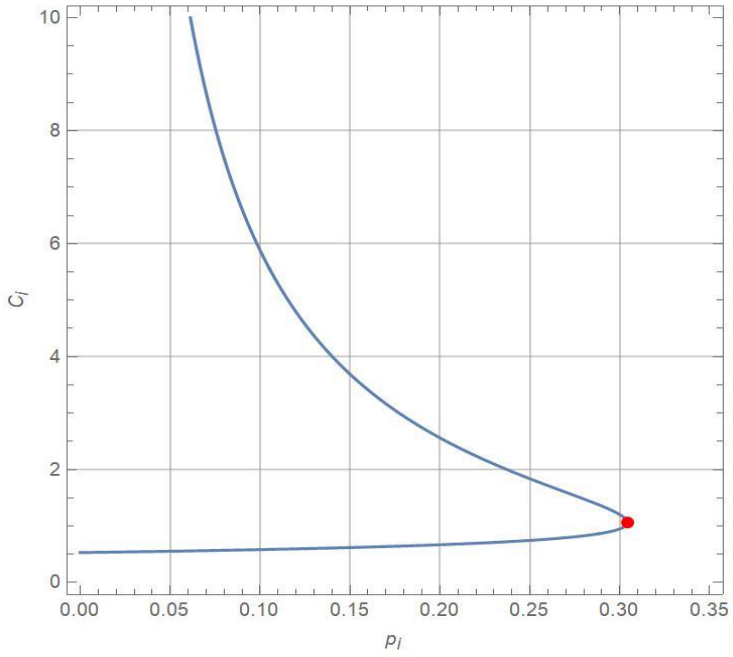


Figure 4. $C_i(p_i)$ bifurcation diagram with the critical point (red point).

The critical value is obtained when the discriminant condition holds, i.e., dI_i/dC_i=0. At the critical condition, the tangent is vertical. At the critical state, the two extrema of the response curve merge, which corresponds to the condition of zero discriminant of Eq. (13) i.e. $q_i^2 - 3\,p_i k_i = 0$. For the Cu model, this condition gives $p_{icr} = 0.3042$. The corresponding critical sediment concentration is $C_{ib} = \frac{q_i}{3p_{icr}} = 1.062$. while the critical Cu concentration in water is obtained from Eq. (25): $I_{icr} = 0.3652$. At this point, the two-fold bifurcation points coalesce and the system reaches the threshold separating the monostable and bistable regimes. Near this critical point, small variations of control parameter p_i may cause large changes in the sediment Cu concentration, leading to abrupt transitions between low- and high-contamination states.

Remark: For the fitted Cu model, $p_i = 0.27$, which is below the critical value $p_{icr} = 0.3042$. Therefore, the system remains in the bistable regime characterized by the existence of two extrema of the stationary response curve (see Figure 2).

At this critical point, the system becomes highly sensitive to parameter variations. Specifically:

- A small variation in control parameter p_i may produce a large change in the sediment concentration Ci, which appears in the bifurcation diagram as a nearly-vertical response near the critical point.
- The stable and unstable equilibrium branches merge and disappear, corresponding to a fold (saddle-node) bifurcation.
- The metal transport process becomes strongly nonlinear, with coexistence of multiple equilibrium states, as illustrated in Figures 2 and 4.

Consequently, the system may undergo an abrupt transition between equilibrium states. The boundary between monostable and bistable regimes is determined by the fold bifurcation points, where the number of real stationary solutions changes.

From a physical perspective, these results indicate that Cu transfer between water and sediment cannot always be described by a gradual proportional relationship. Instead, nonlinear feedback mechanisms may cause a sudden transition from a low-accumulation state to a high-accumulation state, or vice versa, without a continuous intermediate response.

Thus, the vertical tangent in the bifurcation diagram represents the limit of system predictability, where hysteresis effects and abrupt environmental regime shifts may occur.

4.2. Modeling the distribution of Ni between water and sediment based on experimental data

Using the procedure described in Section 3, a model describing the relationship between the Ni input concentration in the water column and its concentration accumulated in the sediment was developed based on experimental data for Ni transport in the South Saskatchewan River [12]. The measured (I_i, C_i) data pairs extracted from the study were (2,12), (4.5,11), (1.5,13), and (3,15), with units of (μg/L, mg/kg).

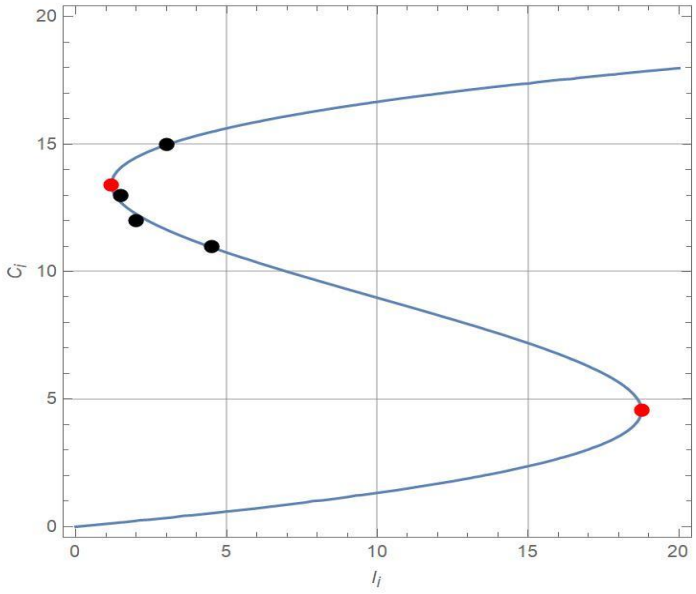


Figure 5. $C_i(I_i)$ diagram for Ni based on the measured values (black points) [12] and critical values (red points).

The model parameters were determined using the least-squares method, yielding k_i=9.280, q_i=1.364, p_i=0.0506. Substituting these values into the proposed model gives the following cubic equation:

$$I_i - 9.280C_i + 1.364\,C_i^2 - 0.0506\,C_i^3 = 0 \tag{27}$$

Figure 5 shows the $C_i(I_i)$ relationship obtained from Eq. (27). Table 3 compares the values calculated using Eq. (27) with the experimental measurements, together with the corresponding relative differences. Since the absolute errors are small, with a maximum deviation of approximately ±0.35, the proposed cubic model provides an excellent description of the observed data.

Table 3. Comparison of measured and calculated Ni concentrations in water.

C_i	I_{im}	I_i	I_{ierr}
12	2.0	2.35	0.1489
11	4.5	4.36	0.0321
13	1.5	1.26	0.1904
15	3.0	3.03	0.0099

Since all parameters in Eq. (27) are positive, the model is compatible with an S-shaped response curve and the occurrence of hysteresis. The fold points of the curve satisfy the condition $\frac{dI_i}{dC_i} = 0$, i.e.,

$$9.280 - 2.728\,C_i + 0.1518\,C_i^2 = 0 \tag{28}$$

The local maximum and minimum values of the Ni concentration in the sediment were obtained by solving Eq. (28). The corresponding values are listed in Table 4 and are marked by red dots in Figure 5.

Table 4. Calculated extremal values of the input Ni concentration I_i and corresponding sediment concentrations C_i.

Type	C_{ib}	I_{ib}
Local maximum	12.6	1.5984
Local minimum	5.40	18.305

Since the measured values are predominantly within the range C_i=11−15, they indeed fall into the region where the upper and lower stable branches of the S-shaped curve may exist. The experimental dataset is highly consistent, enabling accurate predictions based on the S-shaped response curve. Equation (27) enables the sediment Ni concentration C_i to be determined from a measured input concentration I_i, and conversely, the corresponding input concentration I_i can be estimated from a given value of C_i. It should be emphasized, however, that an unambiguous determination of the correct equilibrium state requires knowledge of the system history, since the bistable region exhibits hysteresis.

Figure 6 presents the family of $C_i(I_i)$ diagrams generated from:

$$I_i - 9.280C_i + 1.364\,C_i^2 - \,p_iC_i^3 = 0 \tag{29}$$

for different values of the parameter p_i, illustrating the influence of this parameter on the shape of the equilibrium curve and the occurrence of bistability.

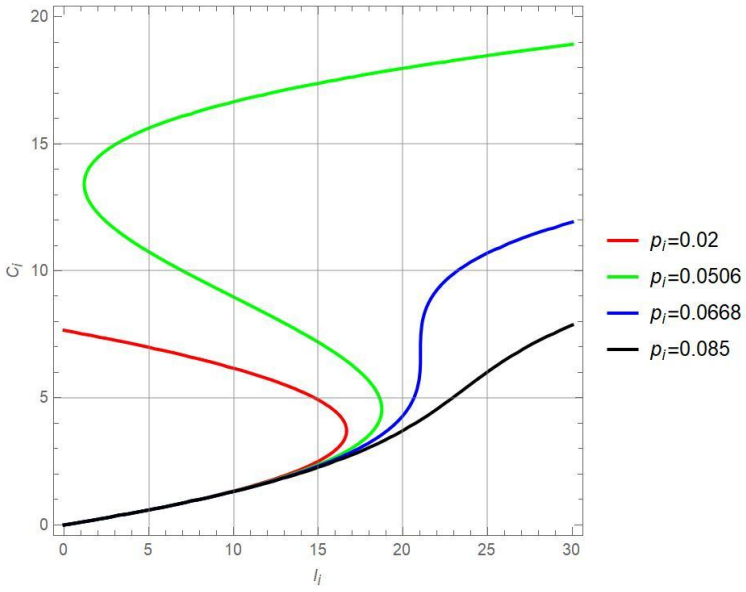


Figure 6. $C_i(I_i)$ diagram for Ni for various values of parameter p_i.

From Figure 6, it can be observed that decreasing p_i weakens the nonlinear cubic contribution, reduces the separation between the fold points, and eliminates the bistable (hysteresis) region, leading to a single-valued monotonic response. At the critical value of pip_p_i, the system loses the ability to support multiple equilibrium states and jump transitions, although the governing relationship remains nonlinear.

To determine the critical value of the parameter p_i, the bifurcation equation corresponding to different values of p_i was analyzed:

$$9.280 - 2.728\,C_i + 3p_i\,C_i^2 = 0 \tag{30}$$

Figure 7 shows the corresponding bifurcation diagram $C_i(p_i)$. The critical point, corresponding to the condition $\mathrm{d}p_i/\mathrm{d}C_i = 0_i$ is obtained as $C_{ibcr} = 6.804$ and $p_{ibcr} = 0.0668$. This point is highlighted by a red dot in Figure 7.

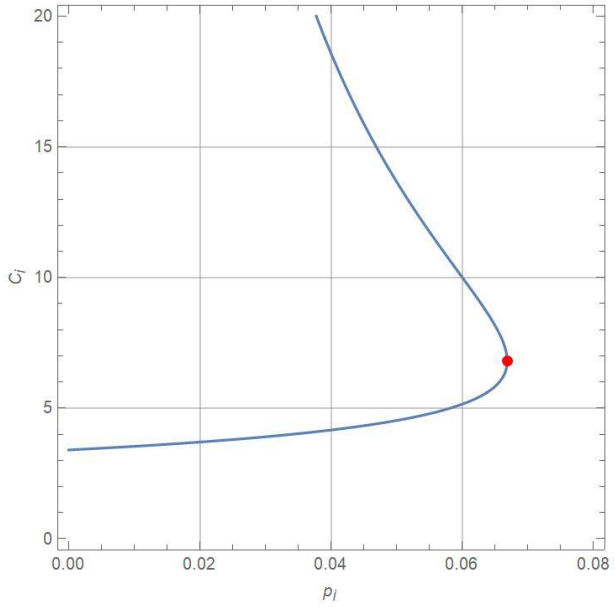


Figure 7. $C_i(\,p_i)$ bifurcation diagram for Ni with the critical point (red point).

Figure 7 demonstrates that two solutions exist for $p_i < p_{ibcr}$, a single critical solution is obtained at $p_{ibcr} = 0.0668$, and no equilibrium solution exists for $p_i > p_{ibcr}$. These findings correspond to the behavior of the bifurcation curves shown in Figure 6.

4.3. Distribution of measured Ni and Cu concentrations in water and sediment with respect to the proposed model: A case study

Measurements of Cu and Ni concentrations in water and sediment were performed at the Danube-Tisa-Danube (DTD) Canal, at the Novi Sad-Savino Selo section near Rumenka, Serbia. Mathematical models had previously been developed based on measurements collected before 2024. The model parameters were determined by least-squares fitting of the experimental data. In this study, the newly measured concentrations were compared with the predictions of the corresponding previously established models. The agreement between measured and calculated values was evaluated by determining the relative errors, providing an independent assessment of the validity and predictive capability of the proposed models for the same monitoring site.

Figure 8 presents the $C_i(I_i)$ model for Cu, analytically described by the following cubic equation:

$$I_i = 2.33913\, C_i - 0.34578\, C_i^2 + 0.013935\, C_i^3 \tag{31}$$

The diagram in Figure 8 exhibits the characteristic S-shaped response with two turning points and a critical point, indicating the existence of multiple equilibrium states.

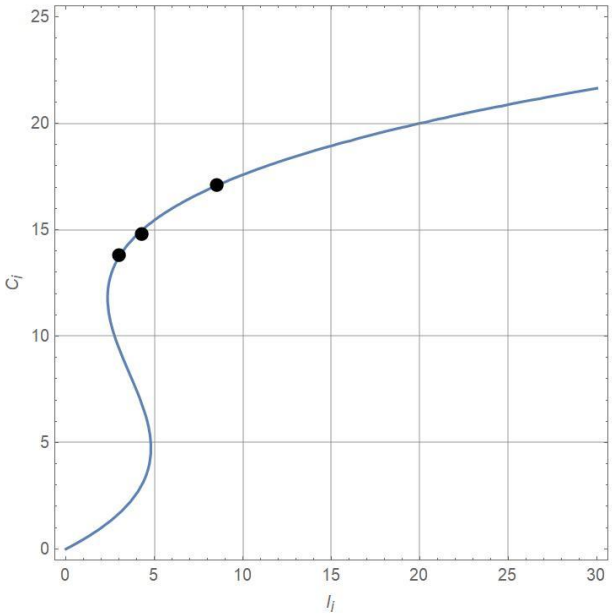


Figure 8. $C_i(I_i)$ diagram for Cu obtained from the proposed cubic model, with newly measured data points (black points)

The newly measured data points, $(C_i,\ I_i)$ = (17.09, 8.54), (14.8, 4.3), and (13.8, 2.99), were superimposed on the existing curve and are shown as black points in Figure 9**.** All newly measured values lie on the upper stable branch of the S-shaped curve. Table 5 compares the measured and model-predicted values of I_i, calculated according to Eq. (31), with the corresponding relative errors.

Table 5. Comparison of measured and calculated Cu concentrations in water.

C_i	I_{im}	I_i	I_{abs}	I_{ierr}
15.10	8.54±1.53	8.5402	0.0002	0.002 %
14.80	4.30±0.70	4.0539	0.2461	5.72 %
15.20	2.38±0.43	3.0550	0.0650	2.17 %

The results demonstrate good agreement between the measured and calculated values. The mean relative error for the three analyzed points is approximately 2.63%, while the maximum absolute error is 0.2461. These results confirm that Equation (31) can be successfully applied to predict the Cu content in sediment based on the corresponding Cu concentration in water at the Danube-Tisa-Danube (DTD) Canal, at the Novi Sad-Savino Selo section near Rumenka, Serbia.

Figure 9 presents the $C_i(\ I_i)$ diagram for Ni, described by the following equation:

$$I_i = 0.150645\ C_i + 2.3614\ 10^{-4} C_i^3 \tag{32}$$

The curve given by Equation (32) was determined based on previous measurements. It was found that the coefficient of the quadratic term in Equation (32) is equal to zero. Therefore, this curve represents a modified S-shaped curve without a critical point.

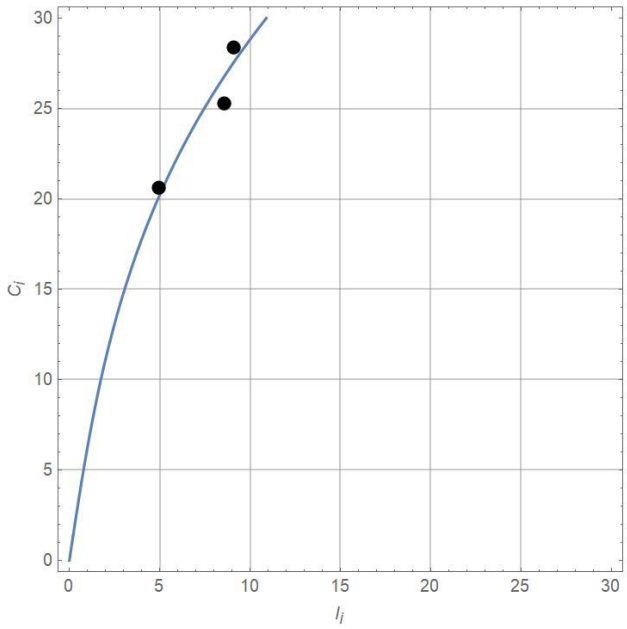


Figure 9. $C_i(I_i)$ diagram for Ni obtained from the proposed cubic model, with newly measured data points (black points).

The newly measured values (C_i, I_i) = (20.6,4.97), (25.3,8.55), and (28.4,9.1) are plotted in Figure 10 and marked as black points. From Figure 10 it can be observed that the measured values are in close proximity to the model curve. Table 6 presents the measured and calculated I_i values, together with the calculated absolute and relative errors.

Table 6. Comparison of measured and calculated Ni concentrations in water

C_i	I_{im}	I_i	I_{abs}	I_{ierr}
16.00	4.97 ± 0.89	5.1676	0.1976	3.98 %
25.30	8.86 ± 1.59	7.6354	0.9146	10.70 %
28.40	8.24 ± 1.48	9.6874	0.5874	6.46 %

For the three analyzed measurement points, the mean relative error is (7.04%), while the maximum absolute error is 0.9. Despite the limited number of validation points, the obtained agreement between the measured and calculated values indicates that the proposed model provides a satisfactory representation of the observed Ni partitioning behavior. Therefore, Equation (32) can be considered a useful predictive tool for estimating Ni content in sediment based on its concentration in water at the Danube-Tisa-Danube (DTD) Canal, at the Novi Sad-Savino Selo section near Rumenka, Serbia. The results confirm that even the simplified cubic model without a critical point can describe the experimentally observed water–sediment relationship and can support the assessment of Ni distribution between the two environmental compartments.

5. Discussion

The proposed nonlinear model provides a unified framework for describing the distribution of heavy metals between the water column and sediment. Unlike conventional linear regression approaches, the cubic formulation captures the nonlinear feedback between the input metal concentration I_i and the sediment concentration C_i, enabling the identification of multiple equilibrium states, fold bifurcations, and hysteresis effects.

The theoretical analysis shows that the existence of an S-shaped response curve is governed by the balance between the linear, quadratic, and cubic terms of the model. The condition for the occurrence of multiple equilibria, $q_i^2 > 3k_i p_i$, defines the parameter region in which two stable equilibrium branches separated by an unstable branch may exist. The fold points obtained from $\frac{dI_i}{dC_i} = 0$ represent critical thresholds at which the system loses stability and undergoes abrupt transitions between different contamination states.

The application to Cu and Ni transport demonstrates the practical significance of this nonlinear behavior. In both cases, the experimental data are accurately represented by the cubic model and are located within the region where an S-shaped response and bistability may occur. Consequently, the same input metal concentration may correspond to different sediment contamination levels depending on the previous evolution of the system. This indicates that the metal partitioning process is not determined exclusively by the current pollution intensity but also depends on the system history.

The obtained results are consistent with previous studies showing that metal partitioning between the aqueous phase and sediments is generally governed by nonlinear adsorption and desorption processes rather than by a strictly proportional relationship. Research on adsorption isotherms has demonstrated that nonlinear formulations can arise from heterogeneous binding sites, saturation effects, and differences in adsorption affinity [14,15]. Our results extend this interpretation by showing that such nonlinear water–sediment relationships may also generate multiple equilibrium states and hysteresis. In addition, the observed threshold behavior is consistent with the broader concept of critical transitions and regime shifts reported for complex aquatic environmental systems [16,17]. However, unlike conventional nonlinear fitting approaches, this study explicitly determines the fold points and critical conditions separating monostable and bistable regimes. This provides an additional interpretation of the nonlinear metal partitioning behavior in terms of potential abrupt transitions and history-dependent responses.

The Cu and Ni models exhibit critical values of the bifurcation parameter p_i that separate bistable and monostable regimes. For the Cu model, the critical condition is obtained as $p_{icr} = 0.3042$, with the corresponding critical sediment concentration $C_{ibcr} = 1.062$ and input concentration $I_{icr} = 0.3652$. For the Ni model, the corresponding critical values are $p_{icr} = 0.0668$ and $C_{ibcr} = 6.804$. These critical points define the transition at which the two-fold points merge and the system lose its ability to sustain multiple equilibrium states. Moreover, the fitted parameter values for both cases, $p_i = 0.27$ for cupper and $p_i = 0.0506$ for Ni, are below their corresponding critical values. Therefore, both calibrated systems operate within the bistable regime characterized by the coexistence of multiple equilibrium solutions and possible hysteresis behavior.

5.1. Environmental interpretation of the critical thresholds

The calculated fold points can be interpreted as site-specific screening thresholds rather than as universal regulatory limits. For the Cu case, the modeled response identifies three concentration regimes: a low-input monostable regime below I_{Cu} =0.27216, a bistable regime between I_{Cu}=0.27216 and 0.34216, and a high-input monostable regime above I_{Cu} =0.34216. The corresponding hysteresis width is ΔI_{Cu} =0.070006. For Ni, the corresponding fold points are I_{Ni} =1.5984 and 18.305, giving a hysteresis width of ΔI_{Ni} =7.20 in the units of the water-column Ni concentration.

Table 7 presents the operational risk zones and hysteresis widths for Cu and Ni, while the corresponding zoning diagrams are shown in Figure 10.

Table 7. Operational risk zones for Cu and Ni.

Metal	Low-contamination monostable zone	Bistable/tipping risk zone	High-contamination monostable zone	Hysteresis width
Cu	$I_i < 0.27216$	$0.27216 \leq I_i \leq 0.34216$	$I_i > 0.34216$	0.070006
Ni	$I_i < 1.5984$	$1.5984 \leq I_i \leq 18.305$	$I_i > 18.305$	16.7066

From an environmental-management perspective, these intervals can be used to define three operational risk zones: The low-input region may be regarded as a lower-risk monostable zone, the interval between the fold points as a tipping-risk or early-warning zone, and the region beyond the upper fold point as a high-contamination zone in which the system is predicted to remain on the high-contamination branch. The bistable interval is particularly important because the sediment state cannot be inferred uniquely from the current aqueous concentration alone and depends on the previous pollution history.

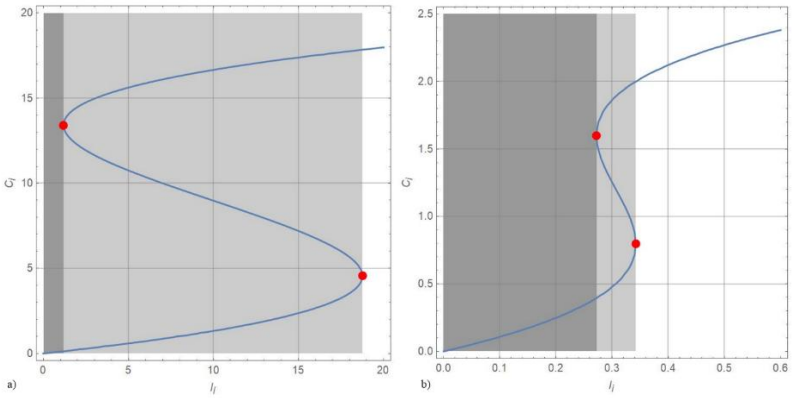


Figure 10. Zoning diagram for: a) Cu and b) Ni, Zone I – low risk zone (dark gray color); Zone II – tipping risk zone (gray color); Zone III – high contamination zone (white color) and the boundary conditions (red points).

These model-derived thresholds should not be interpreted as replacements for legally established water-quality standards. Instead, they provide site-specific nonlinear-response thresholds that can complement regulatory concentration limits. In practical watershed management, the lower fold may be used as an early-warning level, while maintaining aqueous concentrations below the bistable interval may reduce the probability of crossing a transition threshold. Before regulatory application, these thresholds should be independently verified using longer-term monitoring and site-specific physicochemical data.

Based on the data given in Table 7 and the hysteresis indicator $\Delta I = I_{uppr} - I_{lower}$, the relative hysteresis width is obtained as $H = (I_{uppr} - I_{lower})/I_{lower}$; for Cu it is 0.257 and for Ni it is 10.452. Despite the fact that the relative width for the bistable zone is almost 40 times higher for Ni than for Cu it does not mean that the remediation cost is higher. This model does not provide sufficient information to quantify remediation-related costs, which would also require site-specific information on sediment volume, remediation efficiency, treatment duration, recovery kinetics, and associated cost functions.

5.2. Advantages and limitations of the model

The Model considered in this paper is not a complete geomechanical/hydrodynamic model or a regulatory tool, but a reduced-order bifurcation model that provides the site-specific nonlinear screening thresholds.

Within this interpretation, bistability and saddle-node bifurcations are analogous to transitions between alternative states separated by an effective potential barrier. The hysteresis observed in the $C_i(I_i)$ relationship implies that the contamination level may follow different pathways during pollution increase and decrease. Therefore, sediment recovery after pollution reduction may not necessarily occur along the same trajectory as contamination growth, which is relevant for environmental management and remediation strategies.

Within this interpretation, bistability and saddle-node bifurcations are analogous to transitions between alternative states separated by an effective potential barrier. The hysteresis observed in the $C_i(I_i)$ relationship implies that the contamination level may follow different pathways during pollution increase and decrease. Therefore, sediment recovery after pollution reduction may not necessarily occur along the same trajectory as contamination growth, which is an important consideration for environmental management and remediation strategies.

The main advantage of the proposed approach is that it provides information beyond conventional empirical fitting. In addition to reproducing the measured data with small deviations, the model identifies critical thresholds, predicts alternative equilibrium states, and determines conditions under which abrupt changes in sediment contamination may occur. The comparison of Cu and Ni demonstrates that these nonlinear features are not restricted to a particular metal but arise from the proposed cubic transport structure.

However, the model has limitations. Since the cubic formulation describes equilibrium relationships, it does not provide information about the time evolution of the system or the transition rate between different states. Furthermore, within the bistable region, the physically realized equilibrium cannot be uniquely determined from the input concentration alone; additional information

concerning system history, initial conditions, and environmental processes is required. Future developments may include coupling the equilibrium formulation with dynamic transport models and incorporating processes such as sediment resuspension, seasonal variations, and chemical transformations.

A further limitation concerns temporal validation. The available observations provide independent concentration measurements and demonstrate consistency between the model response and measured water–sediment concentrations, but they do not form a sufficiently dense time series through an observed regime transition. Consequently, we validate the equilibrium relationship and the location of the response branches, but we do not validate the duration or rate of transitions between stable states. The bifurcation framework identifies conditions associated with loss of equilibrium stability, whereas the actual temporal evolution of a regime shift depends on kinetic, hydrodynamic, and geochemical processes that are not explicitly resolved here. Future monitoring should therefore combine water and sediment concentrations with pH, TOC, redox potential, suspended solids, flow conditions, and seasonal observations to calibrate and test a dynamic extension of the model.

6. Potential applications and broader significance

Beyond describing the equilibrium relationship between water and sediment contamination, the proposed framework provides a basis for predicting critical transitions in aquatic pollution systems. Unlike conventional approaches that focus mainly on estimating current contamination levels, the bifurcation-based model identifies the conditions under which a gradual increase in pollution input may lead to an abrupt shift toward a highly contaminated sediment state. In this sense, the model can serve as a theoretical foundation for the development of early-warning indicators for environmental regime shifts.

The identification of critical thresholds and hysteresis regions is particularly relevant for sediment management and remediation strategies. Due to history-dependent behavior, a reduction in external pollution input does not necessarily result in an immediate return to the previous contamination state. The proposed approach therefore provides insight into why sediment recovery may exhibit delayed responses and why prevention of crossing critical thresholds is often more effective than remediation after a regime shift has occurred.

Furthermore, the model can be integrated with hydrodynamic and water-quality simulation tools by using predicted pollutant inputs as control parameters for assessing system stability and transition risks. Such integration may improve environmental risk assessment by complementing concentration-based predictions with information about system resilience, stability loss, and potential abrupt changes in contamination regimes.

The main strength and novelty of the proposed framework is therefore not only its ability to reproduce experimental metal concentration data, but its capability to reveal hidden nonlinear mechanisms governing water-sediment interactions. By identifying multistability, hysteresis, and tipping points, the model provides a new perspective for understanding and predicting regime shifts in aquatic pollution dynamics.

Beyond its theoretical contribution, the proposed nonlinear modeling framework may also have relevance for sediment remediation. By identifying critical thresholds, bistability, and abrupt changes

in the equilibrium relationship between metal concentrations in water and sediment, the model provides insight into conditions under which metal partitioning may shift between alternative equilibrium states. This information may contribute to the interpretation of sediment stability and metal mobility, although direct assessment of remobilization would require additional physicochemical, kinetic, and site-specific data. In this context, the framework may provide a theoretical basis for evaluating changes in metal partitioning relevant to remediation technologies such as solidification/stabilization (S/S).

Overall, the results demonstrate that nonlinear bifurcation theory can significantly extend traditional pollutant transport modeling by revealing hidden multistability, regime shifts, and critical transition mechanisms in water–sediment metal contamination systems.

7. Conclusion

In this paper, we provide a unified nonlinear framework for describing and predicting tipping points in sediment contamination dynamics. Unlike conventional linear or purely empirical approaches, the proposed cubic model captures the nonlinear relationship between metal concentration in water and sediment, revealing the existence of multiple equilibrium states, bistability, and hysteresis behavior.

The analysis of Cu and Ni transport demonstrates that the proposed model can accurately represent experimental observations while providing additional information about the underlying nonlinear structure of the system. The obtained $C_i(I_i)$ response curves exhibit S-shaped behavior associated with saddle-node bifurcations, where stable and unstable equilibrium branches coexist. The identified fold points define critical thresholds separating monostable and bistable regimes and determine the conditions under which abrupt transitions between contamination states may occur.

A key contribution of this study is the demonstration that heavy metal partitioning between water and sediment is not always a unique and gradual process. Instead, the system may exhibit multistability, where the same pollution input can correspond to different sediment contamination levels depending on the previous evolution of the system. This history-dependent behavior provides a mathematical explanation for possible regime shifts in sediment contamination dynamics.

The bifurcation analysis further identifies critical values of the control parameter p_i that mark the transition between nonlinear regimes with multiple equilibrium states and regimes with a unique equilibrium response. These critical conditions provide a quantitative measure of the system sensitivity and indicate the possibility of sudden changes caused by relatively small variations of environmental parameters.

Although the proposed model is based on an equilibrium formulation and does not describe the temporal evolution of contamination processes, it provides a valuable theoretical framework for identifying instability thresholds, hysteresis regions, and potential tipping points. Future developments should include coupling the present approach with dynamic transport models and incorporating additional environmental processes such as sediment resuspension, seasonal variability, and chemical transformation mechanisms.

From an environmental-management perspective, the results provide several practical implications. First, the calculated fold points can be used as site-specific early-warning thresholds for

identifying concentration ranges in which the sediment system may become sensitive to abrupt regime shifts. For the case studies, the Cu bistable interval is $0.27216 \leq I_{Cu} \leq 0.34216$, whereas the corresponding Ni interval is $1.5984 \leq I_{Ni} \leq 18.305$. These values should be regarded as model-derived screening thresholds rather than universal regulatory limits and should be recalibrated when environmental conditions or sediment characteristics change.

Second, the existence of hysteresis indicates that reducing the external metal input may not immediately return the sediment to its previous low-contamination state. Consequently, preventive reduction of pollutant inputs before the upper fold threshold is reached may be more effective than relying solely on post-transition remediation. The hysteresis width can also be used as a quantitative indicator of the range of pollution conditions associated with path-dependent sediment behavior.

Finally, the proposed framework can support site-specific watershed monitoring by identifying concentration ranges that warrant increased attention and preventive action. Its practical value lies in complementing water-quality standards with nonlinear screening information, while future site-specific measurements can be used to refine the model parameters and critical thresholds.

Use of AI tools declaration

The authors declare they have not used Artificial Intelligence (AI) tools in the creation of this article.

Acknowledgments

This research is part of the project Innovative sediment management framework for a SUstainNable DANube black Sea system (SUNDANSE), co-funded by the European Union. Views and opinions expressed are however those of the authors only and do not necessarily reflect those of the European Union or the European Climate, Infrastructure and Environment Executive Agency. Neither the European Union nor the granting authority can be held responsible for them.

Conflict of interest

The authors declare no conflicts of interest.

References

1. Bai J, Zhao J, Zhang Z, et al. (2022). Assessment and a review of research on surface water quality modeling. *Ecol Model* 466: 109888. https://doi.org/10.1016/j.ecolmodel.2022.109888
2. Wang Q, Li S, Jia P, et al. (2013) A review of surface water quality models. *Sci World J* 231768. https://doi.org/10.1155/2013/231768
3. Fu B, Merritt WS, Croke BFW, et al. (2019) Catchment scale water quality and erosion models: Review and synthesis. *Environ Model Softw* 114: 75–97. https://doi.org/10.1016/j.envsoft.2018.12.008

4. Geng M, Qian Z, Jiang H, et al. (2024) Assessing the impact of water-sediment factors on water quality to guide river-connected lake water environment improvement. *Sci Total Environ* 912: 168866. https://doi.org/10.1016/j.scitotenv.2023.168866
5. Zhou Y, Wang X, Li W, et al. (2023) Water quality evaluation and pollution source apportionment of surface water in a major city in Southeast China using multi-statistical analyses and machine learning models. *Int J Environ Res Public Health* 20: 881. https://doi.org/10.3390/ijerph20010881
6. Xu X, Lai T, Jahan S, et al. (2022) Water and sediment analyse using predictive models. *arXiv* arXiv:2203.03422.
7. Pimiento MA, Anta J, Torres A (2025) Machine learning predictive modelling for sediment risk indices within an urbanized river channel. *Hazard Adv* 18: 100708. https://doi.org/10.1016/j.hazadv.2025.100708
8. Lai T, Farid F, Kuan Y, et al. (2025) Transfer learning for assessing heavy metal pollution in seaports sediments. *arXiv* arXiv:2506.22096.
9. Luviano Soto I, Concha Sánchez Y, Raya A (2025) Water quality polluted by total suspended solids classified within an artificial neural network approach. *Water Qual Res J* 60: 214–228. https://doi.org/10.2166/wqrj.2024.061
10. Yan T, Shen S-L, Zhou A (2022) Indices and models of surface water quality assessment: Review and perspectives. *Environ Pollut* 308: 119611. https://doi.org/10.1016/j.envpol.2022.119611
11. Shanbehzadeh S, Dastjerdi MV, Hassanzadeh A, et al. (2014) Heavy metals in water and sediment: A case study of Tembi River. *J Environ Public Health* 858720. https://doi.org/10.1155/2014/858720
12. Prajapati S, Sabokruhie P, Brinkmann M, et al. (2023) Modelling transport and fate of copper and nickel across the South Saskatchewan River using WASP–TOXI. *Water* 15: 265. https://doi.org/10.3390/w15020265
13. Nayfeh AH, Mook DT (1975) Nonlinear Oscilations, Eds., New York: John Wiley & Sons.
14. Majd M.M, Kordzadeh-Kermnai V, Ghalandari V et al. (2022) Adsorption isotherm models: A comprehensive and systematic review (2010–2020). *Sci Total Environ* 812: 151334. https://doi.org/10.1016/j.scitotenv.2021.151334
15. Wang J, Guo X (2020) Adsorption isotherm models: Classification, physical meaning, application and solving method. *Chemosphere* 258: 127279. https://doi.org/10.1016/j.chemosphere.2020.127279
16. Kornijów R (2026) Asymmetric responses to resource overload: A bow-tie perspective on lake eutrophication and human obesity. *Theory Biosci* https://doi.org/10.1007/s12064-026-00473-y
17. Zhang H, Li H, Huo S, et al (2025) Navigating tipping points: A complex systems framework for anticipating lake ecosystem collapse. *Fundam Res* https://doi.org/10.1016/j.fmre.2025.07.004
18. USEPA. Method 3051A: Microwave Assisted Acid Digestion of Sediments, Sludges, Soils, and Oils. SW-846. U.S. Environmental Protection Agency, 2007. Available from: https://www.epa.gov/hw-sw846/sw-846-test-method-3051a-microwave-assisted-acid-digestion-sediments-sludges-soils-and

19. USEPA. Method 7000B: Flame Atomic Absorption Spectrophotometry. SW-846. U.S. Environmental Protection Agency, 2007. Available from: https://www.epa.gov/hw-sw846/sw-846-test-method-7000b-flame-atomic-absorption-spectrophotometry
20. USEPA. Method 7010: Graphite Furnace Atomic Absorption Spectrophotometry, Revision 0. SW-846: Test Methods for Evaluating Solid Waste, Physical/Chemical Methods. U.S. Environmental Protection Agency, 2007. Washington, DC, USA. Available from: USEPA. Method 7010: Graphite Furnace Atomic Absorption Spectrophotometry. SW-846. U.S. Environmental Protection Agency, 2007. Available from: https://www.epa.gov/hw-sw846/sw-846-test-method-7010-graphite-furnace-atomic-absorption-spectrophotometry



AIMS Press

© 2026 the Author(s), licensee AIMS Press. This is an open access article distributed under the terms of the Creative Commons Attribution License (https://creativecommons.org/licenses/by/4.0)